

Tracing Ion Migration in Halide Perovskites with Machine Learned Force Fields

Viren Tyagi,^{†,‡} Mike Pols,^{†,‡} Geert Brocks,^{†,‡,¶} and Shuxia Tao^{*,†,‡}

[†]*Materials Simulation & Modelling, Department of Applied Physics and Science Education,
Eindhoven University of Technology, 5600 MB, Eindhoven, The Netherlands*

[‡]*Center for Computational Energy Research, Department of Applied Physics and Science
Education, Eindhoven University of Technology, 5600 MB, Eindhoven, The Netherlands*

[¶]*Computational Chemical Physics, Faculty of Science and Technology and MESA+
Institute for Nanotechnology, University of Twente, 7500 AE, Enschede, The Netherlands*

E-mail: s.x.tao@tue.nl

Abstract

Halide perovskite optoelectronic devices suffer from chemical degradation and current-voltage hysteresis induced by migration of highly mobile charged defects. Atomic scale molecular dynamics simulations can capture the motion of these ionic defects, but classical force fields are too inflexible to describe their dynamical charge states. Using CsPbI_3 as a case study, we develop machine learned force fields from density functional theory calculations and study the diffusion of charged halide interstitial and vacancy defects in bulk CsPbI_3 . We find that negative iodide interstitials and positive iodide vacancies, the most stable charge states for their respective defect type, migrate at similar rates at room temperature. Neutral interstitials are faster, but neutral vacancies are one order of magnitude slower. Oppositely charged interstitials and vacancies, as they can occur in device operation or reverse bias conditions, are significantly slower and can be considered relatively immobile.

Introduction

Halide perovskites are becoming prominent in many optoelectronic applications, including solar cells,¹ light emitting diodes (LEDs),² and photodetectors.³ These materials have an AMX_3 chemical formula, where A is a monovalent inorganic or organic cation (Cs^+ , methylammonium CH_3NH_3^+ , or formamidinium $\text{CH}(\text{NH}_2)^+$), M is a divalent metal cation (Pb^{2+} , or Sn^{2+}), and X is a monovalent halide anion (I^- , Br^- , or Cl^-). Halide perovskites are relatively soft materials. They inherently have a high concentration of intrinsic defects,⁴ which are also quite mobile.⁵

The migration of these defects interferes with device performance. For example, the accumulation of charged defects at the perovskite-electrode interfaces is suggested to cause hysteresis in the current-voltage (I-V) characteristics of these devices.⁶ Migration of defects also leads to the degradation of materials and interfaces. During device operation, defects can trigger redox and chemical decomposition reactions.⁷ Such effects may negatively impact

the optoelectronic properties of the materials, consequently degrading device performance, which is detrimental to the commercialization of perovskite-based optoelectronic devices.⁸

Experimentally, defects are typically characterized through the effects they have on the (thermo)electronic responses of a device^{9–15} Depending on the specific experimental techniques used, it may be possible to assess the charge states and/or the energy levels of the defects present. However, their chemical composition or atomistic structure remains elusive. From general thermodynamic considerations, it is more likely that defects in bulk materials consist of point defects, i.e., single ion vacancies or interstitials, rather than extended or compound defects,¹⁶ which is why both experiment and theory focus on point defects.

Regarding cation defects, no experimental study seems to indicate the presence of Pb-related point defects, or at least, no electronically active, or mobile ones.⁹ Concerning A cation defects opinions are more divided, with some studies suggesting the presence of mobile MA interstitials^{11,12} or vacancies¹² in MAPbI₃, and others finding no evidence for that.^{9,14} In contrast, anion point defects, i.e., halide vacancies and interstitials, are generally considered the dominant mobile species.¹⁰ Whereas some studies insist on the importance of iodide vacancies in lead iodide perovskites,^{9,14} others instead focus on iodide interstitials^{11–13,17}

While it is difficult to assess the chemical and atomistic structure of point defects from experiments, atomistic simulations may help to obtain microscopic understanding. So far, most computational studies simulating the motion of defects have focused on neutral defects.^{18,19} In contrast, the defects characterized in the experiments cited above are charged. Indeed, from first-principles calculations, it follows that under equilibrium conditions, halide interstitials and vacancies are negatively and positively charged, respectively.^{20–24} Moreover, under non-equilibrium conditions, reversed bias in particular, these defects can change their charge state as they capture electrons or holes injected into the perovskite layer.^{13,25}

To describe the motion of iodide defects, one has to deal with these different charge states, and even include the possibility that a charge state changes along the defect migration path, as the position of the defect level that traps the charge depends on the local environment

of the defect. On the one hand, it is very difficult to capture such elements of charge-dependent migration in a classical force field. On the other hand, quantum mechanics-based *ab-initio* molecular dynamics (AIMD) methods can achieve this, but are computationally too expensive to reach the required system sizes and timescales for realistic simulations. This is where machine learned force fields (MLFF), trained using quantum mechanical calculations, offer a promising alternative.

In this study, using CsPbI_3 as a model system, we train accurate machine learned force fields (MLFF) on-the-fly using density functional theory (DFT) calculations for different charge states of halide interstitial and vacancy defects. The accuracy of each MLFF is validated by comparing it with DFT-calculated energies, forces, and the energy barriers of typical migration paths. Subsequently, we conduct long-timescale molecular dynamics (MD) simulations at various temperatures to investigate the diffusion behavior of these defects. Our findings indicate that diffusion coefficients and activation barriers of both defect types (vacancy and interstitial) are significantly impacted by their charge states, with the evolution of structural geometries along the migration path playing a crucial role.

The structures of all defect systems were optimized using the Vienna Ab-Initio Simulation Package (VASP)²⁶ with the PBE-D3-BJ exchange-correlation functional.^{27,28} Following structure optimization, the force fields were trained in VASP, where the training structures were sampled from short-timescale MD runs using Bayesian inference.^{29,30} A combination of a two-body radial descriptor and a three-body angular descriptor, both of similar forms to the smooth overlap of atomic positions (SOAP)^{31,32} descriptor, was used to represent the local chemical environments. A variant of Gaussian approximation potentials (GAP), trained on energies, forces, and stress tensors from DFT calculations,^{29,30,33} was used to generate the force fields. The latter were then used to perform MD runs in VASP.

Similar techniques have been used to study the librational motion of MA cations in MAPbX_3 ,³⁴ and Cs cation rattling in CsPbBr_3 ,³⁵ for instance. Here, we use it to trace the motion of charged iodide point defects in CsPbI_3 . Mean-squared displacements and struc-

tural geometries were analyzed to provide atomic-scale insight into the migration behavior of the ions.

Results

We start by performing DFT calculations to optimize the structures of iodide interstitials and vacancies in three different charge states. They include the most stable intrinsic ones, negatively charged iodide interstitial (I_I^-), and positively charged iodide vacancy (V_I^+) in $CsPbI_3$. By changing the number of electrons in the supercell, other charge states of the iodide interstitial (I_I^0 and I_I^+) and the vacancy (V_I^0 and V_I^-) are created. We observe notable local structural changes for both iodide interstitial (Figure 1a) and iodide vacancy once the charge state changes (Figure 1b), in agreement with previous work.^{20–24}

Band structure calculations are performed to monitor the shift in Fermi level with charge state. These calculations reveal a decrease of the number of electrons (decrease of the Fermi level) is consistent with I_I^- capturing one or two holes, whereas increasing the number of electrons (increasing the Fermi level) leads to V_I^+ capturing one or two electrons. The DFT parameters used for the structure optimizations, as well as the band structures of all defective supercells are given in SI Note 1.

Following structure optimization, we train the MLFFs for all six defect systems at different temperatures over a range from 600K to 750K. The training runs for the defect systems are performed using $2 \times 2 \times 2$ cubic supercells (8 units of $CsPbI_3$) with one iodide point defect. The detailed training procedure for the defective systems can be found in SI Note 2.

To check the accuracy of the force fields, we compare the defect migration barrier calculated with the MLFFs and with DFT, using the climbing image nudged elastic band (CI-NEB) technique;³⁶ the results are shown in Figure 1c-h. The MLFF migration energies are generally in good agreement with the DFT results. Details of the CI-NEB calculations along with all calculated migration barriers are given in SI Note 4.

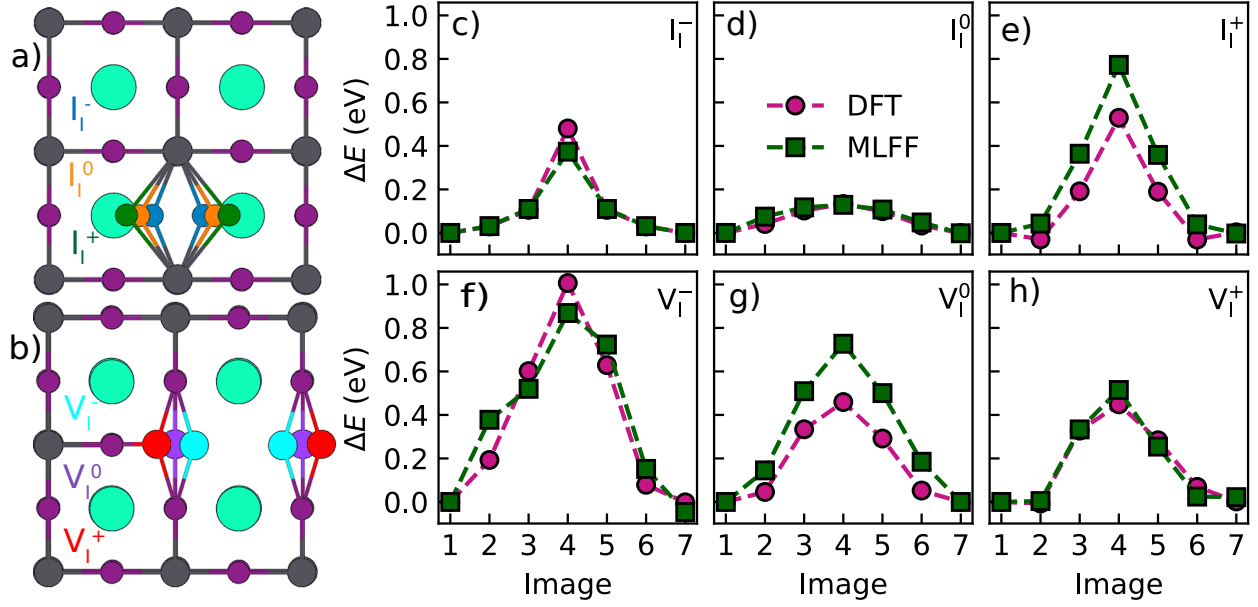


Figure 1: Schematic structures of (a) the iodide interstitial and (b) the iodide vacancy in CsPbI₃ in their different charge states. (c-h) Energies along the NEB migration paths, calculated using DFT and the MLFFs. The points are the calculated values, and the lines guide the eye; the energy of the minima is set to 0.

In addition to energies, we also check the accuracy of these models in predicting forces. We sample 60 structures from MD simulations at 600 K for each defect system and compare the forces calculated using MLFFs with those calculated using DFT, all models have an $R^2 > 0.93$ and a mean absolute error (MAE) $< 0.053 \text{ eV/\AA}$ for these comparisons. For forces acting on the atoms close to the defect environment, all MLFFs have $R^2 > 0.90$ and MAE $< 0.063 \text{ eV/\AA}$, illustrating the high accuracy of these models. The details of these MD runs, the procedure for identifying the defect environments, and the comparison of forces for all MLFFs with DFT can be found in SI Note 4.

Following training and validation, the force fields are used to perform MD simulations on $6 \times 6 \times 6$ cubic supercells (216 units of CsPbI₃) with one iodide point defect at temperatures between 500 K and 600 K. The volume is kept constant during each run with the lattice parameters at the different temperatures extracted from the constant temperature MD runs on pristine CsPbI₃ (see SI Note 3). The temperature range is chosen to ensure a sufficient number of defect migration events within a lattice that is subjected to moderate temperature

fluctuations. Indeed, Our simulations show multiple migration events for all defects, except for V_I^- , where no defect migration was observed at all. The details of the simulation runs are given in SI Note 5.

The diffusion behavior for all five mobile species can be fitted by an Arrhenius relation

$$D = D_0 \exp\left(-\frac{E_a}{k_B T}\right) \quad (1)$$

where k_B is the Boltzmann constant, E_a the activation energy, and D_0 the pre-exponential factor. The fits are shown in Figure 2, and the parameters extracted from the Arrhenius fit are given in Table 1. A full explanation of how the diffusion coefficients are calculated can be found in SI Note 5.

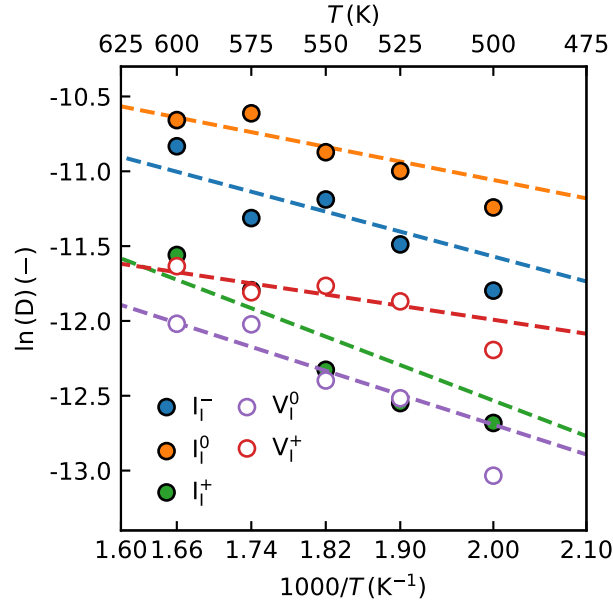


Figure 2: Temperature dependent diffusion coefficients of halide point defects obtained from the MD simulations with the MLFFs. The filled symbols represent halide interstitials, and the open symbols represent halide vacancies. The dashed lines represent the fits to an Arrhenius expression.

Activation energies for diffusion E_a range from 0.12 to 0.29 eV, and are quite dependent on the charge state of the defects. Starting from the iodide interstitial in its most stable charge state, I_I^- ,^{20,24} the activation energy decreases by 0.06 eV if the interstitial catches

Table 1: Activation energies (E_a) and pre-exponential factors (D_0) extracted from the Arrhenius fits, and extrapolated diffusion constants (D_{300K}) at room temperature.

System	E_a (eV)	D_0 ($\times 10^{-3} \text{ cm}^2 \text{ s}^{-1}$)	D_{300K} ($\times 10^{-7} \text{ cm}^2 \text{ s}^{-1}$)
I_I^-	0.22 ± 0.04	1.57 ± 1.39	3.16
I_I^0	0.16 ± 0.02	0.61 ± 0.35	10.14
I_I^+	0.29 ± 0.04	2.54 ± 2.64	0.23
V_I^0	0.28 ± 0.04	1.58 ± 1.44	0.21
V_I^+	0.12 ± 0.04	0.10 ± 0.10	8.22

a hole, I_I^0 , but it increases by 0.07 eV if the interstitial catches two holes, I_I^+ . The iodide vacancy in its most stable charge state, V_I^+ , has the lowest activation energy for diffusion of all cases considered here. The activation energy more than doubles if the vacancy catches an electron, V_I^0 . If the vacancy catches two electrons, V_I^- , we have not observed any diffusion in our simulations, so it is safe to assume that in that case, the activation energy is even higher.

Note that the qualitative trend in activation energies as function of charge state obtained from the NEB calculations, Figure 1, is similar to that obtained from the MD simulations. Quantitatively, however, the NEB values can easily be off by a factor of two, which confirms the notion that NEB calculations might be less suitable for soft materials such as metal halide perovskites, where a representative sampling of migration paths and barriers is difficult to find among the many degrees of freedom.

The pre-exponential factors, D_0 in Table 1, also span quite a wide range of several orders of magnitude. This will be discussed in more detail below. We can use the Arrhenius expression to extrapolate the diffusion coefficients to a lower temperature, at which the infrequency of diffusion events would prohibit a direct simulation. Extrapolated diffusion coefficients (D_{300K}) for room temperature $T = 300 \text{ K}$ are given in Table 1. At this temperature, interstitials and vacancies in their most stable charge states, I_I^- and V_I^+ , have similar diffusion coefficients (3.16 vs. $8.22 \times 10^{-7} \text{ cm}^2 \text{ s}^{-1}$).

At room temperature, the neutral defects, with I_I^- capturing a hole or V_I^+ capturing an electron, behave oppositely. The iodide interstitial I_I^0 migrates faster than I_I^- , while the

iodide vacancy V_I^0 migrates at least one order of magnitude slower than V_I^+ . Finally, I_I^- capturing two holes makes the interstitial I_I^+ much less mobile, whereas V_I^+ capturing two electrons makes the vacancy V_I^- immobile in the present simulations.

Discussion

In a simple model of diffusion of a defect as a random walk on a lattice, the pre-exponential factor can be expressed as

$$D_0 = \frac{d^2}{z} \nu_0, \quad (2)$$

where d is the step size (distance between nearest neighbor defect equilibrium positions), z is the number of possible jump directions from one site, and ν_0 is the attempt frequency. As an example, for an iodide vacancy V_I^+ , $d \approx 4.5 \text{ \AA}$, $z = 8$, and from Table 1 $D_0 = 10^{-4} \text{ cm}^2\text{s}^{-1}$, would give an attempt frequency $\nu_0 = 0.4 \text{ THz}$, which indeed is a typical lattice vibration frequency in CsPbI_3 . We conclude that the pre-exponential factors, extracted from the MD simulations, and listed in Table 1, are within expected physical orders of magnitude.

As for the activation energies, the values listed in Table 1 are smaller than typical values found from NEB calculations, Figure 1. As discussed above, NEB calculations tend to find upper bounds, which in particular for soft materials can be quite far from the actual values. Comparison to experimental values is also not so straightforward. For instance, reported values for the activation energy for diffusion of iodide vacancies range from 0.08 to 0.58 eV, which may be related to the difficulties of extracting this parameter from experiments, as discussed in detail in ref.¹⁰

A fundamental problem is extracting the nature of the diffusing defect from experiment. Some studies focus on iodide vacancies,^{9,10,14} an identification that is typically based upon varying the chemical potential of iodide from iodide poor to rich, and observing the ion conductivity decrease, which is then interpreted as a decrease of iodide vacancy concentration. However, for perovskites, with their charged iodide defects, this approach may be trouble-

some. A change in the iodide chemical potential is compensated under intrinsic conditions by a change in Fermi level. As a result of this the defect formation energies, and therefore their concentrations, are not changed, as explained in ref.²⁴

First-principles calculations often find that the iodide interstitial is more easily formed than the vacancy,^{20–22,24} and should be present in a larger concentration under equilibrium conditions, except under very iodide poor conditions. As an alternative explanation for the decrease in ion conductivity going from iodide poor to rich, we suggest that the intrinsic Fermi level decreases,²⁴ where at some point the iodide interstitials change their charge state from I_I^- to I_I^+ . The latter are much less mobile according to Table 1, which should lead to a lower iodide conductivity. Some experimental studies indeed focus on the role of iodide interstitials^{11–13} Interestingly, the value 0.29 ± 0.06 eV found in ref.¹¹ for the activation energy of the diffusion attributed to the iodide interstitial I_I^- , overlaps with the value 0.22 ± 0.04 eV found from the MD simulations, see Table 1.

A closer examination of the activation energies and pre-exponential factors in Table 1 reveals a relationship, where a larger activation barrier corresponds to a larger pre-exponential factor (figure given in SI Note 6). From Equation 1 this implies that a change in the latter partly compensates for a change in the former, such that the diffusion coefficient is less affected by these changes. As an example, whereas the activation barrier for I_I^- migration is almost double that for V_I^+ migration, see Table 1, the pre-exponential factor is more than an order of magnitude larger. This results in the diffusion coefficients at room temperature D_{300K} for I_I^- and V_I^- being of the same order of magnitude.

Such a (partial) compensation between changes in the activation barrier and in the pre-exponential factor was also reported in experiments by in ref.¹² for $MAPbI_3$, characterizing the migration of MA and I related defects, and categorizing this compensation under the Meyer-Neldel rule. That rule relates the pre-exponential factor of a reaction (or diffusion) rate to the entropy of the transition state, and states that an increase in the energy of the transition state (the activation energy) is accompanied by an increase in its entropy. The

two increases then (partially) compensate one another in their effect on the reaction (or diffusion) rate, see SI Note 6.³⁷⁻³⁹

To help analyze the trends in the diffusion rates, we analyzed the structural geometries along the migration paths, depicted schematically in Figure 3. The iodide interstitial I_I^- in its most stable configuration appears in a characteristic structure, where it doubles the bridge between two Pb ions formed by a lattice iodide, as in Figure 3a.^{20-22,24} The typical migration path for such interstitials then consists of hopping moves of a I atom from one Pb–II–Pb bridge to a neighboring Pb–I–Pb bond to form a double bridge there. The neutral interstitial I_I^0 behaves in a similar way, but its bonding to the Pb atoms is less rigid (figure S9 in SI Note 7), resulting in a slightly lower activation energy and a higher migration rate for I_I^0 .

In contrast, the equilibrium bonding configuration of the positively charged interstitial I_I^+ is quite different. It is not directly bonded to Pb atoms, but instead to two lattice iodides, and forms a linear iodide trimer I_3 , see Figure 3c.^{20-22,24} The diffusion of this interstitial leads to a migration path where the interstitial kicks out a lattice iodide, which then becomes the new interstitial. This migration path has a higher activation energy, resulting in a considerably lower migration rate for I_I^+ compared to the other two charge states of iodide interstitials.

In the case of iodide vacancy, Figure 3d-f, the migration is characterized by an exchange of an I vacancy with an I atom, involving a 90° rotation around the Pb–I bond. The neutral vacancy V_I^0 has a similar migration path, but as a result of V_I^+ capturing an electron, the vacancy is more strongly bonded to the two positively charged Pb surrounding it. Thus, V_I^0 experiences a higher activation barrier than V_I^+ . This effect is even more significant for V_I^- where after adding another electron the bond to the surrounding Pb ions becomes even stronger. This can be observed in a significant shortening of the Pb–Pb bond, where the average distance between these two atoms at 600 K decreases from 5.78 Å and 6.84 Å for V_I^0 and V_I^+ respectively to 3.67 Å for V_I^- . Due to the locked Pb–Pb bond, no migration was observed for V_I^- in the simulated temperature range.

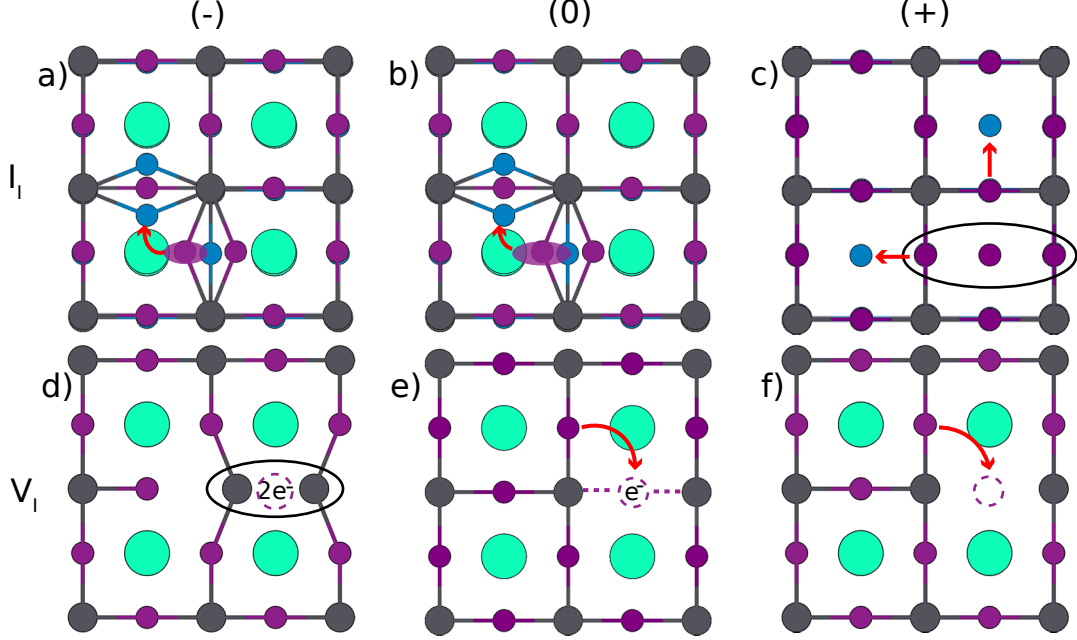


Figure 3: Schematic representations of the diffusion paths of iodide interstitials (a-c) and vacancies (d-f) in their different charge states. The arrows represent the migration directions of the ions.

Conclusions

To summarize, in this work, we trained machine learned force fields for different charge states of iodide interstitial and vacancy defects in CsPbI_3 . Using these force fields we performed long-timescale MD simulations to study the temperature-dependent diffusion behavior of these defects. Our simulations suggest that out of the six investigated species (positive, negative, and neutral interstitials and vacancies), five are mobile. When closely comparing these five mobile species, we found that iodide interstitials and vacancies in their most stable charge states, as they occur under (near) equilibrium conditions (I_I^- , V_I^+), migrate at similar rates at room temperature. Neutral iodide interstitials are somewhat faster, but neutral vacancies are one order of magnitude slower. Oppositely charged interstitials (I_I^+ , V_I^-) and vacancies, such as they can occur in device operating or reverse bias conditions are significantly slower, and can be considered relatively immobile.

Our study demonstrates that machine learned force fields based on quantum mechanical

calculations are an effective tool for studying the dynamical properties of ionic defects. Our findings suggest that the migration rates of defects in halide perovskites undergo notable changes upon capturing charges during device operation and other non-equilibrium conditions. This work paves the way for further studies on the complex interplay and reactions of defects of different types and charges in halide perovskites.

Acknowledgement

The authors thank Henry Kwan for testing the parameters for CI-NEB calculations. V.T. and S.T. acknowledge funding from Vidi (project no. VI.Vid.213.091) from the Dutch Research Council (NWO).

Supporting Information Available

Supporting information will be made available on publication.

References

- (1) Liang, X.; Duan, D.; Al-Handawi, M. B.; Wang, F.; Zhou, X.; Ge, C.-y.; Lin, H.; Zhu, Q.; Li, L.; Naumov, P. et al. The Role of Ionic Liquids in Performance Enhancement of Two-Step Perovskite Photovoltaics. *Sol. RRL* **2023**, *7*, 2200856.
- (2) Lin, K.; Xing, J.; Quan, L. N.; de Arquer, F. P. G.; Gong, X.; Lu, J.; Xie, L.; Zhao, W.; Zhang, D.; Yan, C. et al. Perovskite light-emitting diodes with external quantum efficiency exceeding 20 per cent. *Nature* **2018**, *562*, 245–248.
- (3) Liu, Y.; Zhang, Y.; Yang, Z.; Feng, J.; Xu, Z.; Li, Q.; Hu, M.; Ye, H.; Zhang, X.; Liu, M. et al. Low-temperature-gradient crystallization for multi-inch high-quality perovskite single crystals for record performance photodetectors. *Mater. Today* **2019**, *22*, 67–75.

- (4) Wang, F.; Bai, S.; Tress, W.; Hagfeldt, A.; Gao, F. Defects engineering for high-performance perovskite solar cells. *npj flex. electron.* **2018**, *2*, 22.
- (5) Ball, J. M.; Petrozza, A. Defects in perovskite-halides and their effects in solar cells. *Nat. Energy* **2016**, *1*, 16149.
- (6) Li, J.; Dong, Q.; Li, N.; Wang, L. Direct Evidence of Ion Diffusion for the Silver-Electrode-Induced Thermal Degradation of Inverted Perovskite Solar Cells. *Adv. Energy Mater.* **2017**, *7*, 1602922.
- (7) Yu, X.; Wang, Y.; Gao, P. The Effect of Redox Reactions on the Stability of Perovskite Solar Cells. *ChemPhotoChem* **2023**, *7*, e202200311.
- (8) Chen, X.; Sun, Z.; Cai, B.; Li, X.; Zhang, S.; Fu, D.; Zou, Y.; Fan, Z.; Zeng, H. Substantial Improvement of Operating Stability by Strengthening Metal-Halogen Bonds in Halide Perovskites. *Adv. Funct. Mater.* **2022**, *32*, 2112129.
- (9) Senocrate, A.; Moudrakovski, I.; Kim, G. Y.; Yang, T.-Y.; Gregori, G.; Grätzel, M.; Maier, J. The nature of ion conduction in methylammonium lead iodide: a multimethod approach. *Angew. Chem.* **2017**, *129*, 7863–7867.
- (10) Senocrate, A.; Maier, J. Solid-state ionics of hybrid halide perovskites. *J. Am. Chem. Soc.* **2019**, *141*, 8382–8396.
- (11) Futscher, M. H.; Lee, J. M.; McGovern, L.; Muscarella, L. A.; Wang, T.; Haider, M. I.; Fakharuddin, A.; Schmidt-Mende, L.; Ehrler, B. Quantification of ion migration in $\text{CH}_3\text{NH}_3\text{PbI}_3$ perovskite solar cells by transient capacitance measurements. *Mater. Horiz.* **2019**, *6*, 1497–1503.
- (12) Reichert, S.; An, Q.; Woo, Y.-W.; Walsh, A.; Vaynzof, Y.; Deibel, C. Probing the ionic defect landscape in halide perovskite solar cells. *Nat. Commun.* **2020**, *11*, 6098.

- (13) Ni, Z.; Jiao, H.; Fei, C.; Gu, H.; Xu, S.; Yu, Z.; Yang, G.; Deng, Y.; Jiang, Q.; Liu, Y. et al. Evolution of defects during the degradation of metal halide perovskite solar cells under reverse bias and illumination. *Nat. Energy* **2022**, *7*, 65–73.
- (14) Tammireddy, S.; Reichert, S.; An, Q.; Taylor, A. D.; Ji, R.; Paulus, F.; Vaynzof, Y.; Deibel, C. Temperature-dependent ionic conductivity and properties of iodine-related defects in metal halide perovskites. *ACS Energy Lett.* **2021**, *7*, 310–319.
- (15) Ghasemi, M.; Guo, B.; Darabi, K.; Wang, T.; Wang, K.; Huang, C.-W.; Lefler, B. M.; Taussig, L.; Chauhan, M.; Baucom, G. et al. A multiscale ion diffusion framework sheds light on the diffusion–stability–hysteresis nexus in metal halide perovskites. *Nat. Mater.* **2023**, *22*, 329–337.
- (16) Xue, H.; Vicent-Luna, J. M.; Tao, S.; Brocks, G. Compound Defects in Halide Perovskites: A First-Principles Study of CsPbI₃. *J. Phys. Chem. C* **2023**, *127*, 1189–1197.
- (17) Thiesbrummel, J.; Shah, S.; Gutierrez-Partida, E.; Zu, F.; Peña-Camargo, F.; Zeiske, S.; Diekmann, J.; Ye, F.; Peters, K. P.; Brinkmann, K. O. et al. Ion-induced field screening as a dominant factor in perovskite solar cell operational stability. *Nat. Energy* **2024**, 1–13.
- (18) Balestra, S. R.; Vicent-Luna, J. M.; Calero, S.; Tao, S.; Anta, J. A. Efficient modelling of ion structure and dynamics in inorganic metal halide perovskites. *J. Mater. Chem. A* **2020**, *8*, 11824–11836.
- (19) Pols, M.; Brouwers, V.; Calero, S.; Tao, S. How fast do defects migrate in halide perovskites: insights from on-the-fly machine-learned force fields. *Chem. Commun.* **2023**, *59*, 4660–4663.
- (20) Meggiolaro, D.; Motti, S. G.; Mosconi, E.; Barker, A. J.; Ball, J.; Andrea Riccardo Perini, C.; Deschler, F.; Petrozza, A.; De Angelis, F. Iodine chemistry determines the defect tolerance of lead-halide perovskites. *Energy Environ. Sci.* **2018**, *11*, 702–713.

- (21) Meggiolaro, D.; De Angelis, F. First-principles modeling of defects in lead halide perovskites: best practices and open issues. *ACS Energy Lett.* **2018**, *3*, 2206–2222.
- (22) Xue, H.; Brocks, G.; Tao, S. First-principles calculations of defects in metal halide perovskites: A performance comparison of density functionals. *Phys. Rev. Mater.* **2021**, *5*, 125408.
- (23) Zhang, X.; Turiansky, M. E.; Shen, J.-X.; Van de Walle, C. G. Defect tolerance in halide perovskites: A first-principles perspective. *J. Appl. Phys.* **2022**, *131*, 090901.
- (24) Xue, H.; Brocks, G.; Tao, S. Intrinsic defects in primary halide perovskites: A first-principles study of the thermodynamic trends. *Phys. Rev. Mater.* **2022**, *6*, 055402.
- (25) Motti, S. G.; Meggiolaro, D.; Barker, A. J.; Mosconi, E.; Perini, C. A. R.; Ball, J. M.; Gandini, M.; Kim, M.; De Angelis, F.; Petrozza, A. Controlling competing photochemical reactions stabilizes perovskite solar cells. *Nat. Photonics* **2019**, *13*, 532–539.
- (26) Kresse, G.; Furthmüller, J. Efficient iterative schemes for ab initio total-energy calculations using a plane-wave basis set. *Phys. Rev. B* **1996**, *54*, 11169–11186.
- (27) Perdew, J. P.; Burke, K.; Ernzerhof, M. Generalized Gradient Approximation Made Simple. *Phys. Rev. Lett.* **1996**, *77*, 3865–3868.
- (28) Grimme, S.; Ehrlich, S.; Goerigk, L. Effect of the damping function in dispersion corrected density functional theory. *J. Comput. Chem.* **2011**, *32*, 1456–1465.
- (29) Jinnouchi, R.; Lahnsteiner, J.; Karsai, F.; Kresse, G.; Bokdam, M. Phase transitions of hybrid perovskites simulated by machine-learning force fields trained on the fly with Bayesian inference. *Phys. Rev. Lett.* **2019**, *122*, 225701.
- (30) Jinnouchi, R.; Karsai, F.; Kresse, G. On-the-fly machine learning force field generation: Application to melting points. *Phys. Rev. B* **2019**, *100*, 014105.

- (31) Bartók, A. P.; Kondor, R.; Csányi, G. On representing chemical environments. *Phys. Rev. B* **2013**, *87*, 184115.
- (32) Jinnouchi, R.; Karsai, F.; Verdi, C.; Asahi, R.; Kresse, G. Descriptors representing two- and three-body atomic distributions and their effects on the accuracy of machine-learned inter-atomic potentials. *J. Chem. Phys.* **2020**, *152*, 234102.
- (33) Bartók, A. P.; Payne, M. C.; Kondor, R.; Csányi, G. Gaussian Approximation Potentials: The Accuracy of Quantum Mechanics, without the Electrons. *Phys. Rev. Lett.* **2010**, *104*, 136403.
- (34) Bokdam, M.; Lahnsteiner, J.; Sarma, D. D. Exploring Librational Pathways with on-the-Fly Machine-Learning Force Fields: Methylammonium Molecules in MAPbX₃ (X = I, Br, Cl) Perovskites. *J. Phys. Chem. C* **2021**, *125*, 21077–21086.
- (35) Lahnsteiner, J.; Bokdam, M. Anharmonic lattice dynamics in large thermodynamic ensembles with machine-learning force fields: CsPbBr₃, a phonon liquid with Cs rattlers. *Phys. Rev. B* **2022**, *105*, 024302.
- (36) Henkelman, G.; Uberuaga, B. P.; Jónsson, H. A climbing image nudged elastic band method for finding saddle points and minimum energy paths. *J. Chem. Phys.* **2000**, *113*, 9901–9904.
- (37) Meyer, W. v.; Neldel, H. Relation between the energy constant and the quantity constant in the conductivity–temperature formula of oxide semiconductors. *Z. tech. Phys* **1937**, *18*, 588–593.
- (38) Du, P.; Li, N.; Ling, X.; Fan, Z.; Braun, A.; Yang, W.; Chen, Q.; Yelon, A. Optimizing the Proton Conductivity with the Isokinetic Temperature in Perovskite-Type Proton Conductors According to Meyer–Neldel Rule. *Adv. Energy Mater.* **2022**, *12*, 2102939.

- (39) Takamure, N.; Sun, X.; Nagata, T.; Ho-Baillie, A.; Fukata, N.; McKenzie, D. R. Thermodynamic Interpretation of the Meyer-Neldel Rule Explains Temperature Dependence of Ion Diffusion in Silicate Glass. *Phys. Rev. Lett.* **2022**, *129*, 175901.